Check for updates

Geophysical Research Letters

RESEARCH LETTER
10.1029/2025GL117291

A 400-Year Sediment Record of Tsunamis in Qi'ao Island, Centered at Guangdong-Hong Kong-Macao Greater Bay Area

Long Tan[1,2], Yang Zhou[3], Chuanhui Song[1,2], Lei Xing[1,2], Longhai Zhu[4], Nan Wang[5], Yonggang Jia[6], Zhe Su[7], Qiang Qiu[8], Baojin Wu[1,2], Cecilia McHugh[9], and Rui Bao[1,2]

[1]Key Laboratory of Marine Chemistry Theory and Technology, Frontiers Science Center for Deep Ocean Multispheres and Earth System, Ministry of Education, Innovation Center for Ocean Carbon Neutrality, Ocean University of China, Qingdao, China, [2]Laboratory for Marine Ecology and Environmental Science, Qingdao National Laboratory for Marine Science and Technology, Qingdao, China, [3]Guangzhou Marine Geological Survey, Guangzhou, China, [4]College of Marine Geosciences, Ocean University of China, Qingdao, China, [5]Key Lab of Submarine Geosciences and Prospecting Techniques, Frontiers Science Center for Deep Ocean Multispheres and Earth System, Ministry of Education and College of Marine Geosciences, Ocean University of China, Qingdao, China, [6]Shandong Provincial Key Laboratory of Marine Environment and Geological Engineering, Ocean University of China, Qingdao, China, [7]National Institute of Natural Hazards, Ministry of Emergency Management of China, Beijing, China, [8]Key Laboratory of Ocean and Marginal Sea Geology, South China Sea Institute of Oceanology, Chinese Academy of Sciences, Guangzhou, China, [9]Earth and Environmental Sciences, Queens College, City University of New York, New York, NY, USA

Abstract Identifying tsunamis and determining inundation extent is critical for coastal hazard assessment. We identify potential tsunami deposits in the Guangdong-Hong Kong-Macao Greater Bay Area that occurred in 1555 ± 135 CE using a multidisciplinary approach. The inverted ^{14}C ages of organic matter in sediments, consistent dating of shells, and increased coarse-grained content imply that a rapid, high-energy event occurred in the Greater Bay Area. The presence of shell fossils, bimodal grain size distributions, the absence of laminar textures, and an increased concentration of the marine-derived biomarker brassicasterol in the sediment sequence collectively suggest that these sediments are likely deposits from a tsunami. Tsunami simulations further indicate that larger earthquakes from the Manila Trench could be responsible for this tsunami in the Greater Bay Area. Our findings provide preliminary evidence that tsunamis may be a critical natural hazard concern for the densely populated Greater Bay Area.

Plain Language Summary Our research provides evidence of a tsunami that hit the Guangdong-Hong Kong-Macao Greater Bay Area about 400 years ago. In the QAD-ZK3 core, the anomalously young organic matter (OM) ^{14}C ages, consistent shell dating, and the coarser grain size suggest that a high-energy event happened. This layer of sediment is interpreted as tsunami deposits based on abundant shells, two sequences that get finer toward the top, fine sand with poor sorting, no lamination textures, and more marine OM. Using ^{14}C dating on OM and shells and $^{210}Pb_{ex}$ age, we found that the tsunami happened around 1555 ± 135 CE. The results from tsunami modeling are consistent with the geological record of the tsunami in the Greater Bay Area. Our study shows that tsunamis caused by the Manila Trench are a potential natural disaster for the crowded Greater Bay Area.

Key Points:

- Multiproxy evidence suggests depositional events in the QAD-ZK3 core that occurred in 1555 ± 135 CE may correspond to a tsunami
- Tsunami modeling suggests that Manila Trench-triggered earthquakes could be the cause of the tsunami deposit found in the Greater Bay Area
- Our findings offer preliminary evidence that future tsunamis may threaten the densely populated Greater Bay Area

Supporting Information:

Supporting Information may be found in the online version of this article.

Correspondence to:

R. Bao, L. Xing, L. Zhu and N. Wang,
baorui@ouc.edu.cn;
xinglei@ouc.edu.cn;
zhulonghai@ouc.edu.cn;
wn@ouc.edu.cn

Citation:

Tan, L., Zhou, Y., Song, C., Xing, L., Zhu, L., Wang, N., et al. (2025). A 400-year sediment record of tsunamis in Qi'ao Island, centered at Guangdong-Hong Kong-Macao Greater Bay Area. *Geophysical Research Letters*, *52*, e2025GL117291. https://doi.org/10.1029/2025GL117291

Received 29 MAY 2025
Accepted 13 AUG 2025

Author Contributions:

Conceptualization: Rui Bao
Methodology: Chuanhui Song, Lei Xing, Nan Wang, Baojin Wu
Resources: Yang Zhou, Lei Xing
Writing – original draft: Long Tan, Chuanhui Song
Writing – review & editing: Longhai Zhu, Yonggang Jia, Zhe Su, Qiang Qiu, Cecilia McHugh, Rui Bao

© 2025 The Author(s).
This is an open access article under the terms of the Creative Commons Attribution-NonCommercial License, which permits use, distribution and reproduction in any medium, provided the original work is properly cited and is not used for commercial purposes.

1. Introduction

Tsunamis are primarily triggered by submarine earthquakes, which can lead to sediment resuspension and severe damage to inundated areas. In the 2004 Indian Ocean Tsunami, the M_w 9.2 Sumatra-Andaman earthquake triggered the tsunami that devastated Southeast Asia, causing more than 2 km of inland inundation on Phra Thong Island and massive loss of life (Jankaew et al., 2008). Similarly, driven by the tectonically active Manila Subduction Zone (MSZ), destructive tsunami waves can be generated and propagated toward the coastal regions of South China (Li et al., 2022; Megawati et al., 2009). The Guangdong-Hong Kong-Macao Greater Bay Area is located on the coast of South China and accommodates over 86.9 million residents. Moreover, the Littoral Fault Zone (LFZ), as the boundary fault between the South China sub-plate and the South China Sea (SCS) sub-plate, has generated four large crustal earthquakes in the past 400 years (Li et al., 2024; Xia et al., 2020), which increases the potential tsunami threat. Historical records suggest that approximately 50 potential tsunami events have

19448007, 2025, 19, Downloaded from https://agupubs.onlinelibrary.wiley.com/doi/10.1029/2025GL117291 by Ocean University Of China, Wiley Online Library on [03/10/2025]. See the Terms and Conditions (https://onlinelibrary.wiley.com/terms-and-conditions) on Wiley Online Library for rules of use; OA articles are governed by the applicable Creative Commons License

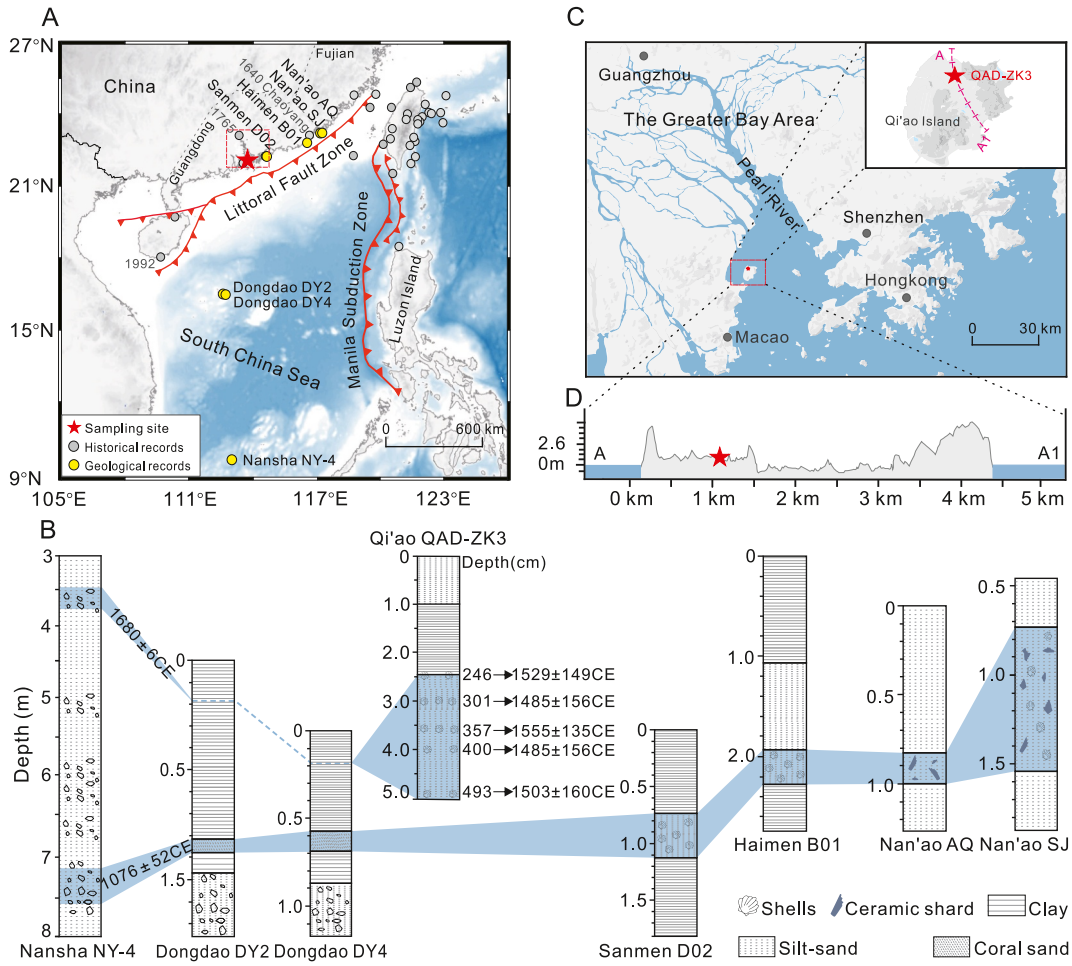

Figure 1. Overview of sampling sites and tsunami records. (a) Tectonic setting and historical tsunami records. Gray dots of the historical tsunami records (Lau et al., 2010) and modified from (Li et al., 2022). Yellow dots indicate possible geological tsunami deposit records. (b) Correlated sites of tsunami geologic deposit records, including the 1024 CE Dongdao tsunamis (Sun et al., 2013), the 1076 CE Nan'ao Island tsunamis (Yang et al., 2019), the 1048–1108 CE Sanmen tsunamis and Haimen tsunamis (Wang et al., 2023), and the 1680 CE storm or tsunami event recorded on the Nansha Island (Yu et al., 2009). (c) Our sampling site is located in the Greater Bay Area. (d) Topographic features of the QAD-ZK3 core.

occurred in the SCS region since 1000 CE (Lau et al., 2010). However, only the tsunami of 1076 CE has been corroborated by extensive geological deposits found in the Dongdao and Nansha Islands within the SCS, as well as in Haimen, Sanmen, and Nan'ao Islands along the South China coast (Sun et al., 2013; Wang et al., 2023; Yang et al., 2019; Yu et al., 2009). Other paleotsunamis reported in historical accounts lack supporting geological evidence (Figure 1a). To enhance our comprehension of tsunami hazards along the mainland coast of South China, it is essential to accurately identify tsunami sequences and inundation extents to mitigate the significant risks associated with potential future tsunamis.

Sedimentological investigations of the 1076 CE tsunami deposits show the presence of biogenic debris, sand layers, and normal grading sequences across multiple study sites (Figure 1b), which serve as preliminary criteria for identifying tsunami deposits. A fundamental problem is that tsunamis and storm surges have similar inflow patterns (Phantuwongraj & Choowong, 2012; Shinozaki, 2021), both with high-energy flows scouring the beach area and then resuspending these materials into terrestrial environments. Thus, sedimentary features such as shell fossils and sand layers may also occur in storm deposits (Zhou et al., 2019), limiting the reliability of sedimentological proxies to distinguish between tsunami and storm deposits. Biomarkers are persistent and source-specific (Alpar et al., 2012), offering a reliable solution for separating variations in marine and terrestrial organic matter (OM) inputs during event deposition. In this context, marine-sourced short-chained n-alkane biomarkers

19448007, 2025, 19, Downloaded from https://agupubs.onlinelibrary.wiley.com/doi/10.1029/2025GL117291 by Ocean University Of China, Wiley Online Library on [03/10/2025]. See the Terms and Conditions (https://onlinelibrary.wiley.com/terms-and-conditions) on Wiley Online Library for rules of use; OA articles are governed by the applicable Creative Commons License

have been applied to the 2011 Tohoku-oki tsunami deposits by linking to elevated marine or coastal inputs during the inundation (Bellanova et al., 2020; Konechnaya et al., 2022). In coastal and estuarine environments, storm deposits generally consist of a combination of marine sediments transported by storm surges and fluvial sediments resulting from precipitation (Yao et al., 2023; Zheng et al., 2017). This process may lead to an increase in terrestrial OM inputs. Further research needs to apply multiple proxies to identify tsunami deposits and assess the effectiveness of biomarkers in differentiating paleotsunami deposits from those formed by storms.

Establishing a reliable chronology is crucial for tsunami research, as it facilitates the correlation of tsunami histories across extensive regions. Radiocarbon dating of shells found within tsunami deposits may yield ages that are either older than or contemporaneous with the actual timing of the event (Ishizawa et al., 2017). The OM above and below the tsunami deposits can further refine depositional ages, as ^{14}C ages from these layers can be used to constrain the younger and older ages of the tsunami deposit (Ishizawa et al., 2020). However, tsunami deposits are source-dependent and consist of reworked sediments (Goff et al., 2012). The number, type, and preservation conditions of the dating material and the reworking of the sediments by the tsunami will affect the ^{14}C results. The ^{210}Pb dating, with a half-life of 22.26 years, is useful for dating sedimentation processes over a timescale of up to 100 years (Appleby & Oldfield, 1978). The excess ^{210}Pb ($^{210}Pb_{ex}$) decay profile can also aid in identifying whether co-deposited OM and shell ^{14}C results are affected by sedimentary processes. Employing a multi-dating approach enhances the establishment of a robust chronological framework and facilitates the determination of the regional distribution of tsunami deposits associated with the same event.

This study investigates whether tsunamis threaten the Greater Bay Area by identifying and dating tsunami deposits. Based on the QAD-ZK3 core, we integrate multiproxy evidence from topographic features, sedimentology, and organic geochemistry to identify tsunami deposits. The ^{14} C dating of OM and shells and $^{210}Pb_{ex}$ are applied to determine the chronological framework and to link the tsunami records in the SCS. Tsunami modeling is employed to trace potential tsunami sources and provides a primary reference for coastal hazard assessment in South China.

2. Materials and Methods

2.1. Regional Background and Sampling

The Qi'ao Island is located at the center of the Greater Bay Area, facing Hong Kong and Shenzhen to the east and Macao to the south (Figure 1c). Hydrodynamic conditions around Qi'ao Island started to weaken around 2000 years ago, and fluvial sediments from the Pearl River were gradually accumulated (Li et al., 2001). The construction of seawalls and the planting of mangroves in the 1990s further accelerated sediment accumulation on this island. Because the SCS is adjacent to active tropical cyclones in the Northwest Pacific Ocean, 1–2 typhoons land in Guangdong Province annually (Chan & Shi, 2000). The average spring tidal range in the Pearl River estuary varies from 0.86 m at the mouth to 1.57 m at the head of the estuary (Huang et al., 2004). During the summer fieldwork of 2019, we collected a 5-m-long sediment core with a diameter of 7 cm from Qi'ao Island (22.43°N, 113.63°E, 1.3 m above sea level) using a Russian Peat Borer. The QAD-ZK3 core is located within the Mangrove Nature Reserve and is a considerable distance from human settlements (Figures 1c and 1d). The sedimentary core is composed of light brownish-gray silty clay sediments, exhibiting no significant deformations in sedimentary bedding, and demonstrates a nearly 100% sampling rate.

2.2. Methods

The 14 OM and shell samples were analyzed using accelerator mass spectrometry at Beta Analytic Laboratory and the Woods Hole Oceanographic Institution. The ^{14}C ages of OM and shell were converted to calendar years using the Marine20 calibration data set (Heaton et al., 2020) with a DeltaR value of -23 ± 42 (Yoneda et al., 2007). Calibrated calendar ages are provided in Table S1 in Supporting Information S1. The $^{210}Pb_{ex}$ concentration in the sediment was measured with an HPGe (GWL-120-15-XLB-AWT, ORTEC) type γ-energy spectrometer. The $^{210}Pb_{ex}$ chronology for the QAD-ZK3 core is established using the constant initial concentration ratio model (Appleby & Oldfield, 1978), which assumes constant deposition rates throughout the deposition (see Text S1 in Supporting Information S1).

Sediments were pretreated with an excess of 10% HCl and 30% H_2O_2 for 24 hr to remove carbonates and OM, followed by adding sodium metaphosphate solution. Then, these samples were measured using a laser Particle

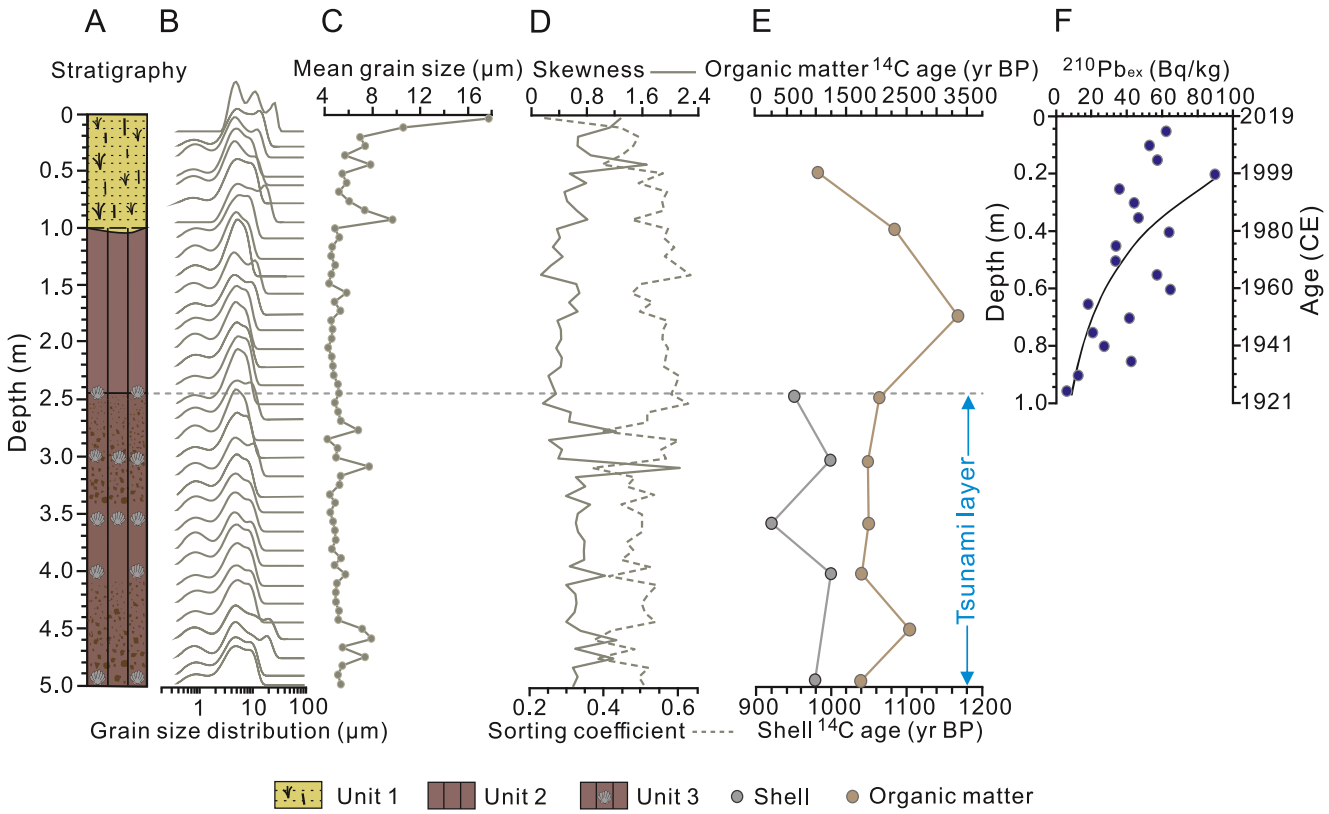

Figure 2. Lithological profile of core QAD-ZK3. (a) Stratigraphy of three sedimentary units. (b–d) Grain size parameters include grain size distribution curves, mean grain size, skewness, and sorting coefficients. (e) AMS ^{14}C ages between organic matter and shells. (f) ^{210}Pb$_{ex}$ age-depth model.

Size Analyzer (Mastersizer 2000, UK) for grain size parameters. After carbonate removal, total organic carbon (TOC), total nitrogen, and stable isotope ($\delta^{13}C$, $\delta^{15}N$) were quantified by an EA-IsoLink elemental analyzer coupled to a MAT253 plus isotope ratio mass spectrometer. Biomarkers were extracted by sonicating samples four times with dichloromethane and methanol (DCM: MeOH; 3:1, v/v) after adding quantitative internal standards of C_{19} *n*-alkanol. Extracts were dried under the N_2 stream and then hydrolyzed with 6% KOH in MeOH for 12 hr. Sterol and n-alkanol components were eluted with DCM: MeOH (95:5, v/v) after removal of the n-alkanes by N-hexane and dried under the N_2 stream. The extracts were derivatized with DCM and N, O-bis (trimethylsilyl)-trifluoroacetamide (BSTFA) at 70°C for 1 hr (Xing et al., 2011). The content of brassicasterol, dinosterol, and n-alkanol was calculated from the peak area results of Gas Chromatography (GC, Agilent 6890N). Tsunami generation and propagation from different earthquake sources in the SCS (the M_w 9.0 MSZ and M_w 7.5 LFZ) are simulated using the Cornell Multi-grid Coupled Tsunami (COMCOT) model (Text S2 in Supporting Information S1), which uses linear/nonlinear shallow-water equations to simulate tsunami wave propagation in deep oceans or near shore (Wang & Power, 2011).

3. Results and Discussion

3.1. The Multiproxy Characteristics of Tsunami Deposits on Qi'ao Island

According to the lithological profile, the QAD-ZK3 core is divided into three sedimentary units (Figure 2a). A stratigraphic unconformity exists at the base of Unit 1, which consists of yellow silt with highly variable grain size ranging from 4.8 to 17.7 μm and multi-peaked grain size distribution curves containing plant debris (Figures 2b and 2c). Unit 2 is characterized by well-sorted reddish-brown silt (average 4.8 μm) with unimodal distribution curves. Bulk grain size parameters of Unit 2 sediments indicate deposition in a relatively stable hydrodynamic environment. The bottom Unit 3 contains abundant shell fragments and exhibits two fining-upward sequences at 250–340 and 410–490 cm. An increase in grain size and skewness with the lowest sorting coefficients is also observed in Unit 3 sediments (Figure 2d), which suggests that it consists of poorly sorted fine sand fractions.

19448007, 2025, 19, Downloaded from https://agupubs.onlinelibrary.wiley.com/doi/10.1029/2025GL117291 by Ocean University Of China, Wiley Online Library on [03/10/2025]. See the Terms and Conditions (https://onlinelibrary.wiley.com/terms-and-conditions) on Wiley Online Library for rules of use; OA articles are governed by the applicable Creative Commons License

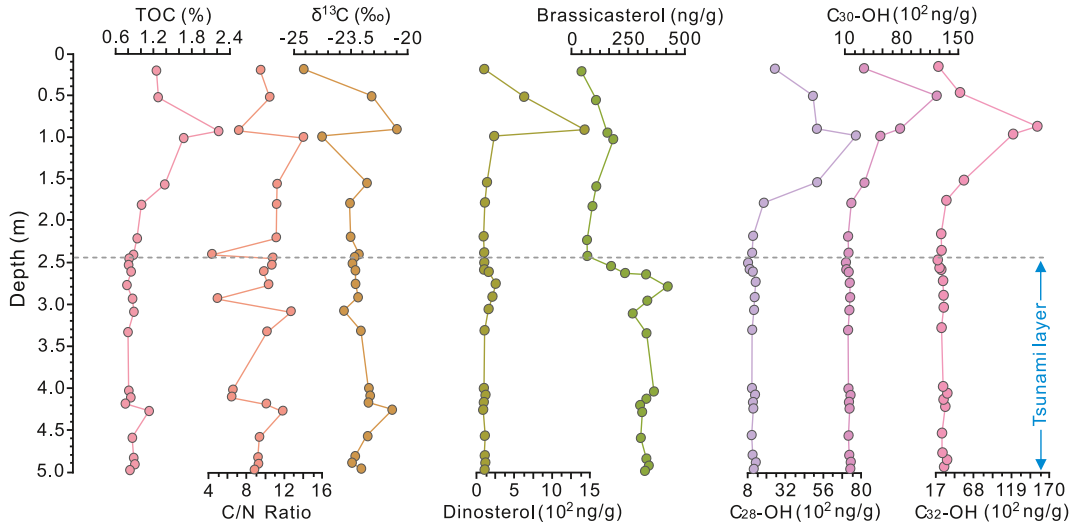

Figure 3. Organic geochemical proxies. Biomarker brassicasterol and dinosterol can be used as proxies for marine organic matter. The n-alkanol C_{28}-OH, C_{30}-OH, and C_{32}-OH contents indicate the input of terrestrial higher plants.

Radiocarbon dating of bulk OM yields ^{14}C ages ranging from 1040 ± 30 to 3350 ± 30 years BP for Units 1 and 2 sediments (Figure 2e), following a normal age-depth pattern. The normal $^{210}Pb_{ex}$ decay profile further suggests that the sedimentary process in Unit 1 is continuous (Figure 2f). In contrast, deeper sediments in Unit 3 show anomalously younger OM ages from 1744 ± 111 to 2580 ± 30 years BP, indicating a chronological inversion. Shells from Unit 3 also consistently yield ^{14}C ages of 920–1000 (±30) yr BP. Downcore variations in OM and shell ^{14}C ages support that Unit 3 sediment undergoes rapid reworking and depositional processes and has shifted to a relatively high-energy hydrodynamic condition.

Further organic geochemical analysis is conducted to characterize the palaeoenvironments of sedimentary units. Unit 3 exhibits significantly lower TOC of 0.86%, with C/N ratios ranging from 4.90 to 12.67 and $\delta^{13}C$ values between −20.68‰ and −22.82‰ (Figure 3). These organic geochemical parameters in Unit 3 are consistent with the C/N ratios and $\delta^{13}C$ values of marine sediment in Pearl River Delta (Zong et al., 2010). In Unit 2 sediments, C/N ratios (average 11.7) and $\delta^{13}C$ values (average −22.5‰) exhibit less variation, indicating a stable hydrodynamic environment with increased terrestrial OM. The dual-carbon ($\delta^{13}C$ and C/N) mass balance mixing model also shows that the proportion of marine OM in Unit 3 sediments increased to 71.5%, while the soil OM declined from 29.7% in Units 1 and 2 to 22.0% (Figure S1 in Supporting Information S1). Biomarker composition in the QAD-ZK3 core reveals a similar variation pattern in OM sources. Brassicasterol is derived from diatoms, and dinosterol from dinoflagellates (Lattaud et al., 2017), reflecting marine OM contributions. Phytoplankton communities in the Pearl River are dominated by diatoms (Li et al., 2014), which makes brassicasterol a more reliable indicator of marine OM than dinosterol. Long-chain n-alkanols (C_{28}-OH, C_{30}-OH, and C_{32}-OH) are characteristic components of epidermal waxes in higher plants (Eglinton & Hamilton, 1967). In Unit 3 sediment, terrestrial C_{28}-OH, C_{30}-OH, and C_{32}-OH contents reach the lowest values, while marine-derived brassicasterol increases significantly to 427 ng/g (Figure 3), revealing a marine depositional environment. The terrestrial biomarkers are relatively high in Units 1 and 2 sediments, with the highest values of 7,686, 12,166, and 15,421 ng/g. Conversely, the marine-derived brassicasterol is in a low range of 49–186 ng/g. Combined with the inverted OM ^{14}C ages, consistent dating of shells, poorly sorted grain size, and the significantly increased marine OM, Unit 3 sediments are deposited under high-energy marine conditions, likely reflecting perturbations from coastal currents, sea level changes, or extreme events.

On the East China Sea inner shelf, sediments affected by coastal currents display unimodal grain size distributions associated with a stable hydrodynamic condition (Xiao et al., 2005). Unit 3 sediments show bimodal grain size distribution curves with relatively minor variations in the ^{14}C age ranges of shells (Figures 2b and 2e), implying a rapid event of limited duration. The abrupt decline in marine brassicasterol concentrations is observed at the boundary between Unit 3 and Unit 2 (Figure 3), suggesting a rapid fluctuation in marine OM input only. If sea-level changes influence the hydrodynamic conditions in Unit 3, one would expect the marine and terrestrial

19448007, 2025, 19, Downloaded from https://agupubs.onlinelibrary.wiley.com/doi/10.1029/2025GL117291 by Ocean University Of China, Wiley Online Library on [03/10/2025]. See the Terms and Conditions (https://onlinelibrary.wiley.com/terms-and-conditions) on Wiley Online Library for rules of use; OA articles are governed by the applicable Creative Commons License

19448007, 2025, 19, Downloaded from https://agupubs.onlinelibrary.wiley.com/doi/10.1029/2025GL117291 by Ocean University Of China, Wiley Online Library on [03/10/2025]. See the Terms and Conditions (https://onlinelibrary.wiley.com/terms-and-conditions) on Wiley Online Library for rules of use; OA articles are governed by the applicable Creative Commons License

biomarkers to exhibit gradual variations corresponding to gradual changes in sea level. Besides, the sea level in the Pearl River Delta has remained stable at its contemporary level for the past 1500 years (Xiong et al., 2018; Zhang et al., 2024). We infer that the sediments in Unit 3 may result from high-energy depositional events, such as inland flooding, tropical cyclones, or tsunamis. Only the increased marine OM input and abundant shell fragments suggest that Unit 3 is unlikely to be attributed to extreme inland flooding.

During tsunami waves wash over coastal areas, sediments and organisms are suspended and then transported to the terrestrial environment. The free settling of suspended material is related to a decrease in flow velocity, forming the fining-upward sequence (Goff et al., 2012; Watanabe et al., 2018). Thus, tsunami deposits typically exhibit multiple normal gradings, are rich in shells, and have highly variable grain sizes. In our case, Unit 3 sediments reveal the presence of abundant shell fragments, two fining upward sequences, poorly sorted fine sand, and the absence of lamination textures. Combined with the significantly increased levels of marine-sourced brassicasterol in this sequence. We propose that Unit 3 is most likely to be tsunami deposits, and the tsunami resulting in marine invasions and elevated marine OM inputs can only contribute to the variation in brassicasterol content. The two fining-upward sequences in Unit 3 may record two individual surging tsunami waves. Conversely, tropical cyclones typically cause increased runoff in the Pearl River (Wang et al., 2021) and transport considerable amounts of suspended sediments to be deposited in coastal and estuarine environments, in which the sediments will show an increase in terrestrial OM level and decreased marine productivity (Chen et al., 2017; Yao et al., 2023). Biomarkers provide critical insights for identifying paleotsunami deposits, in which only the marine-derived brassicasterol is significantly elevated in tsunami deposits, reflecting enhanced marine OM inputs from tsunami-induced transport of marine or coastal material. We summarize the tsunami proxies used to differentiate tsunami and storm deposits on Qi'ao Island (Table S2 in Supporting Information S1).

3.2. Chronological Constraints of Tsunami Events

To decipher the timing of the potential tsunami deposits in the QAD-ZK3 core, we dated shell and bulk OM ^{14}C ages above and within Unit 3. The ^{14}C ages of shells above, within, and below the tsunami deposits are remarkably consistent at 1529 ± 149, 1555 ± 135, and 1503 ± 156 CE (Table S1 in Supporting Information S1), suggesting that these shells died simultaneously during the tsunami run-up phase. Thus, the ^{14}C ages of shells may be contemporary with the actual date of the tsunami event, which probably occurred around the youngest age of 1555 ± 135 CE. In addition, the $^{210}Pb_{ex}$ reveals that 0–100 cm in Unit 1 is dated to 1921–2019 CE (Figure 2f), with an accumulation rate of 1.03 cm/yr. According to the constant accumulation rate of 1.03 cm/yr, we estimate an approximate date of 1651 CE at 357 cm. The $^{210}Pb_{ex}$ age is close to the shell ^{14}C age at 357 cm (1555 ± 135 CE), suggesting that shell materials can provide a relatively accurate age of the tsunami event.

The ^{14}C ages of the OM in Unit 3 are consistently older than the results from co-layered shells (Figure 2e). Sediments and OM around Qi'ao Island are mainly from the Pearl River input (Qiao et al., 2021; Yu et al., 2010). Considering that OM in the Pearl River sediments exhibits a significantly older ^{14}C age of 1940 ± 30 years BP (Liu et al., 2017). The "old" OM from the Pearl River is deposited along with sediments into the QAD-ZK3 core, which may be responsible for consistently older bulk OM ^{14}C ages than co-layered shells. Interestingly, the OM ^{14}C ages of Unit 3 are anomalously younger than Units 1 and 2 and show synchronous variation characteristics with marine brassicasterol content. This implies that fresh and younger marine OM transported by the tsunami waves may have contributed to the anomalous younger OM ^{14}C age in Unit 3.

The ^{14}C age of shells suggests that the tsunami deposits in the QAD-ZK3 core range from 1420 CE to 1696 CE. During this period, the historical tsunami database shows that only the 1640 or 1641 CE Chaoyang tsunami events occurred in Guangdong Province (Lau et al., 2010). Similarly, sedimentary records indicate that a potential tsunami may have occurred in the Nansha Islands in 1680 ± 6 CE (Yu et al., 2009). Under this phenomenon, the tsunami deposits found in the Greater Bay Area, the Chaoyang tsunami, and the Nansha tsunami records likely represent a tsunami with widespread impacts on the SCS region.

3.3. Impact of Tsunamis on the Greater Bay Area and Asian Coastal Cities

The MSZ and LFZ are identified as potential trigger zones for large earthquakes in the SCS (Li et al., 2022; Qiu et al., 2019; Zhu et al., 2024). Here, we conduct a detailed tsunami hazard assessment for the Greater Bay Area using the COMCOT, which compares representative earthquake scenarios of the MSZ and LFZ (Text S2). In worst-case scenarios involving the MSZ (M_w 9.0), all simulations predict a maximum surface elevation of

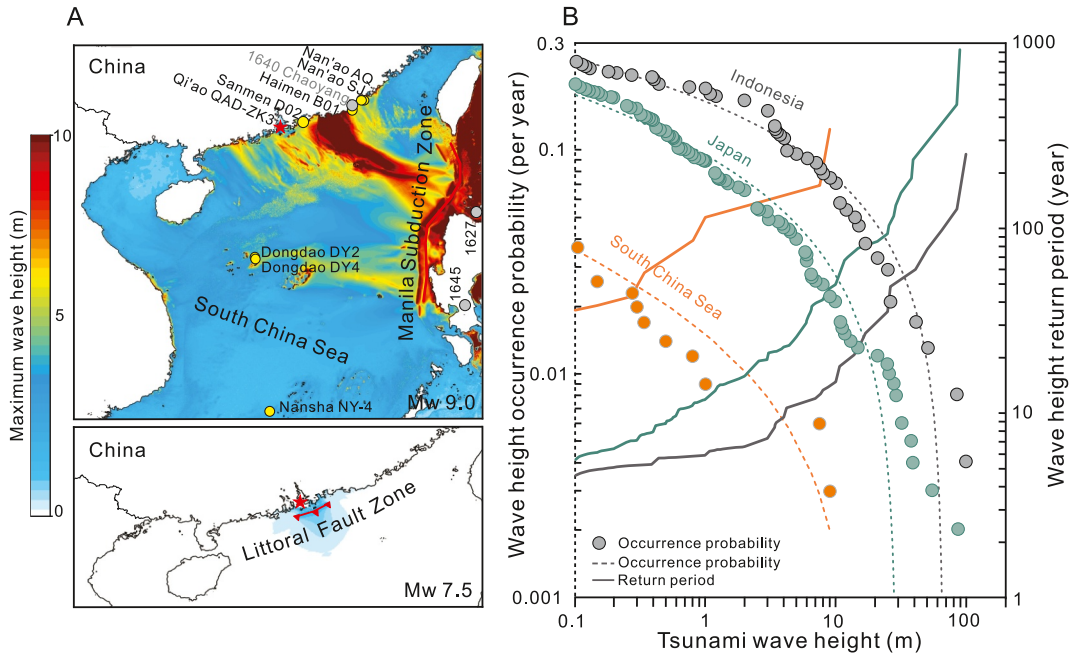

Figure 4. (a) Spatial distributions of maximum surface elevation simulated by the Manila Subduction Zone (upper) and the Littoral Fault Zone (lower). (b) The probability analysis of tsunami hazards in Japan, Indonesia, and South China Sea since 1000 CE.

approximately 2–7.75 m in the Greater Bay Area (Figure 4a), with inundation hazards mainly occurring in Macao and Hong Kong. It is worth noting that the tsunami waves rapidly decay to 2–3.5 m after entering the estuary due to the blocking effects of the Wanshan Islands outside the Pearl River estuary. In contrast, the LFZ (M_w 7.5) is projected to generate a maximum surface elevation of only 1–2 m, primarily affecting the area of the outer continental shelf off the Pearl River mouth (Figure 4a). The maximum surface elevation generated by the MSZ can explain this tsunami deposit in the Greater Bay Area. Moreover, historical tsunami data from the National Oceanic and Atmospheric Administration National Centers for Environmental Information (NCEI 2024, https://ngdc.noaa.gov/hazard/tsu.shtml) show that two potential tsunamis in the MSZ region occurred in 1627 CE (M_w 7.5) and 1645 CE (M_w 8.0), as shown in Figure 4a. This provides contemporaneous geological evidence with the tsunamis deposit in the Greater Bay Area, which aligns with the worst-case modeling scenarios for the MSZ. Combined with the two widespread tsunami deposits occurring in 1076 ± 35 CE and 1640 ± 48 CE at various locations within the SCS (Sun et al., 2013; Wang et al., 2023; Yang et al., 2019; Yu et al., 2009) and modeling results underscores the vulnerability of the Greater Bay Area and the coastal regions of South China to severe and widespread tsunami damage from the Manila Trench-triggered tsunami.

Examining historical tsunami records is essential for understanding tsunami phenomena and performing accurate risk assessments. Three major subduction zones in Asia are believed to bring significant tsunami threats to the surrounding coastal cities (Goto et al., 2021; Jankaew et al., 2008; Li et al., 2022), including the Sunda Trench, the Manila Trench, and the Japan Trench. Historical tsunami data from the NCEI database indicate that Japan has experienced a notably high frequency of tsunami events, with at least 247 confirmed occurrences since 1000 CE, followed by 70 events in Indonesia. Using these historical tsunami data, we conducted a tsunami risk assessment using the probabilistic tsunami hazard analysis (PTHA) (see Text S3 in Supporting Information S1 for details of the methodology). The PTHA provides a wave height return period by calculating the probability of at least one tsunami occurring per year with tsunami amplitudes exceeding a certain specified wave height value (Geist & Parsons, 2006; Ren et al., 2014). The findings indicate that Japan, Indonesia, and the SCS region are at high risk for tsunami hazards, with return periods for tsunami wave heights exceeding 7.75 m being 40.3, 12.7, and 201.3 years, respectively (Figure 4b). Since the SCS region has limited historical records of tsunamis, and available wave height data lacks accuracy, complicating the analysis of these events, this may create a false impression that the Greater Bay Area is not at risk of tsunami threats. In fact, our sedimentary records and

19448007, 2025, 19, Downloaded from https://agupubs.onlinelibrary.wiley.com/doi/10.1029/2025GL117291 by Ocean University Of China, Wiley Online Library on [03/10/2025]. See the Terms and Conditions (https://onlinelibrary.wiley.com/terms-and-conditions) on Wiley Online Library for rules of use; OA articles are governed by the applicable Creative Commons License

modeling results indicate that tsunamis may still pose a significant threat to the Greater Bay Area, underscoring the urgent need for enhanced disaster preparedness measures moving forward.

Conflict of Interest

The authors declare no conflicts of interest relevant to this study.

Data Availability Statement

All data and supplementary materials in this study are available in Tan et al. (2025). Historical tsunami data is available from the National Centers for Environmental Information (https://ngdc.noaa.gov/hazard/tsu.shtml).

Acknowledgments
This study is funded by the National Natural Science Foundation of China (42525604 and 42450135), the Fundamental Research Funds for the Central Universities (202042010), and the National Key R&D Program of China (Grant 2022YFC2803800). We thank the assistance of the R/V "HAI YANG DI ZHI ER HAO" implementing the open research cruise NORC2024-302, supported by the Shiptime Sharing Project (42349302). We acknowledge Linlin Li and Fating Li for their support in tsunami simulation.

References

Alpar, B., Ünlü, S., Altınok, Y., Özer, N., & Aksu, A. (2012). New approaches in assessment of tsunami deposits in Dalaman (SW Turkey). *Natural Hazards*, *63*(1), 181–195. https://doi.org/10.1007/s11069-010-9692-5

Appleby, P. G., & Oldfield, F. (1978). The calculation of lead-210 dates assuming a constant rate of supply of unsupported ^{210}Pb to the sediment. *Catena*, *5*(1), 1–8. https://doi.org/10.1016/S0341-8162(78)80002-2

Bellanova, P., Frenken, M., Reicherter, K., Jaffe, B., Szczuciński, W., & Schwarzbauer, J. (2020). Anthropogenic pollutants and biomarkers for the identification of 2011 Tohoku-oki tsunami deposits (Japan). *Marine Geology*, *422*, 106117. https://doi.org/10.1016/j.margeo.2020.106117

Chan, J. C. L., & Shi, J.-E. (2000). Frequency of typhoon landfall over Guangdong province of China during the period 1470–1931. *International Journal of Climatology*, *20*(2), 183–190. https://doi.org/10.1002/(SICI)1097-0088(200002)20:2<183::AID-JOC479>3.0.CO;2-U

Chen, L., Liu, J., Xing, L., Krauss, K. W., Wang, J., Xu, G., & Li, L. (2017). Historical changes in organic matter input to the muddy sediments along the Zhejiang-Fujian Coast, China over the past 160 years. *Organic Geochemistry*, *111*, 13–25. https://doi.org/10.1016/j.orggeochem.2017.06.003

Eglinton, G., & Hamilton, R. J. (1967). Leaf epicuticular waxes. *Science*, *156*(3780), 1322–1335. https://doi.org/10.1126/science.156.3780.1322

Geist, E. L., & Parsons, T. (2006). Probabilistic analysis of tsunami hazards. *Natural Hazards*, *37*(3), 277–314. https://doi.org/10.1007/s11069-005-4646-z

Goff, J., Chagué-Goff, C., Nichol, S., Jaffe, B., & Dominey-Howes, D. (2012). Progress in palaeotsunami research. *Sedimentary Geology*, *243–244*, 70–88. https://doi.org/10.1016/j.sedgeo.2011.11.002

Goto, K., Ishizawa, T., Ebina, Y., Imamura, F., Sato, S., & Udo, K. (2021). Ten years after the 2011 Tohoku-oki earthquake and tsunami: Geological and environmental effects and implications for disaster policy changes. *Earth-Science Reviews*, *212*, 103417. https://doi.org/10.1016/j.earscirev.2020.103417

Heaton, T. J., Köhler, P., Butzin, M., Bard, E., Reimer, R. W., Austin, W. E. N., et al. (2020). Marine20–The marine radiocarbon age calibration curve (0–55,000 cal BP). *Radiocarbon*, *62*(4), 779–820. https://doi.org/10.1017/RDC.2020.68

Huang, Z., Zong, Y., & Zhang, W. (2004). Coastal inundation due to sea level rise in the pearl river Delta, China. *Natural Hazards*, *33*(2), 247–264. https://doi.org/10.1023/B:NHAZ.0000037038.18814.b0

Ishizawa, T., Goto, K., Yokoyama, Y., & Goff, J. (2020). Dating tsunami deposits: Present knowledge and challenges. *Earth-Science Reviews*, *200*, 102971. https://doi.org/10.1016/j.earscirev.2019.102971

Ishizawa, T., Goto, K., Yokoyama, Y., Miyairi, Y., Sawada, C., Nishimura, Y., & Sugawara, D. (2017). Sequential radiocarbon measurement of bulk peat for high-precision dating of tsunami deposits. *Quaternary Geochronology*, *41*, 202–210. https://doi.org/10.1016/j.quageo.2017.05.003

Jankaew, K., Atwater, B. F., Sawai, Y., Choowong, M., Charoentitirat, T., Martin, M. E., & Prendergast, A. (2008). Medieval forewarning of the 2004 Indian Ocean tsunami in Thailand. *Nature*, *455*(7217), 1228–1231. https://doi.org/10.1038/nature07373

Konechnaya, O., Bellanova, P., Frenken, M., Reicherter, K., & Schwarzbauer, J. (2022). Evaluation of organic indicators derived from extractable, hydrolysable and macromolecular organic matter in sedimentary tsunami deposits. *Marine Geology*, *443*, 106671. https://doi.org/10.1016/j.margeo.2021.106671

Lattaud, J., Kim, J.-H., De Jonge, C., Zell, C., Sinninghe Damsté, J. S., & Schouten, S. (2017). The C_{32} alkane-1,15-diol as a tracer for riverine input in coastal seas. *Geochimica et Cosmochimica Acta*, *202*, 146–158. https://doi.org/10.1016/j.gca.2016.12.030

Lau, A. Y. A., Switzer, A. D., Dominey-Howes, D., Aitchison, J. C., & Zong, Y. (2010). Written records of historical tsunamis in the northeastern south China Sea-challenges associated with developing a new integrated database. *Natural Hazards and Earth System Sciences*, *10*(9), 1793–1806. https://doi.org/10.5194/nhess-10-1793-2010

Li, C., Lei, Y., He, W., & Dai, Z. (2001). Land-ocean interaction in modern delta formation and development: A case study of the pearl river Delta, China. *Science in China, Series B: Chemistry*, *44*(S1), 63–71. https://doi.org/10.1007/BF02884810

Li, F., Li, L., Yu, F., Huang, K., & Switzer, A. D. (2024). Forward numerical investigation of potential tsunami deposits in the South China Sea: A case study of Nan'ao Island. *Marine and Petroleum Geology*, *160*, 106612. https://doi.org/10.1016/j.marpetgeo.2023.106612

Li, L., Liu, J., He, J., & Wang, H. (2014). Factors affecting the abundance and community structure of the phytoplankton in northern South China Sea in the summer of 2008: A biomarker study. *Chinese Science Bulletin*, *59*(10), 981–991. https://doi.org/10.1007/s11434-013-0106-4

Li, L., Qiu, Q., Li, Z., & Zhang, P. (2022). Tsunami hazard assessment in the South China Sea: A review of recent progress and research gaps. *Science China Earth Sciences*, *65*(5), 783–809. https://doi.org/10.1007/s11430-021-9893-8

Liu, Z., Zhao, M., Sun, H., Yang, R., Chen, B., Yang, M., et al. (2017). "Old" carbon entering the South China Sea from the carbonate-rich pearl river basin: Coupled action of carbonate weathering and aquatic photosynthesis. *Applied Geochemistry*, *78*, 96–104. https://doi.org/10.1016/j.apgeochem.2016.12.014

Megawati, K., Shaw, F., Sieh, K., Huang, Z., Wu, T. R., Lin, Y., et al. (2009). Tsunami hazard from the subduction megathrust of the South China Sea: Part I. Source characterization and the resulting tsunami. *Journal of Asian Earth Sciences*, *36*(1), 13–20. https://doi.org/10.1016/j.jseaes.2008.11.012

National Geophysical Data Center/World Data Service. (2024). *NCEI/WDS global historical tsunami database*. NOAA National Centers for Environmental Information. https://doi.org/10.7289/V5PN93H7

19448007, 2025, 19, Downloaded from https://agupubs.onlinelibrary.wiley.com/doi/10.1029/2025GL117291 by Ocean University Of China, Wiley Online Library on [03/10/2025]. See the Terms and Conditions (https://onlinelibrary.wiley.com/terms-and-conditions) on Wiley Online Library for rules of use; OA articles are governed by the applicable Creative Commons License

Phantuwongraj, S., & Choowong, M. (2012). Tsunamis versus storm deposits from Thailand. *Natural Hazards*, *63*(1), 31–50. https://doi.org/10.1007/s11069-011-9717-8

Qiao, Y., Liu, J., Cao, L., Rahaman Khan, M. H., Xu, X., & Tan, L. (2021). Contribution of continuously stable sediment input to the formation of the pearl river Delta since the middle Holocene. *Quaternary International*, *598*, 78–89. https://doi.org/10.1016/j.quaint.2021.05.010

Qiu, Q., Li, L., Hsu, Y. J., Wang, Y., Chan, C. H., & Switzer, A. D. (2019). Revised earthquake sources along Manila trench for tsunami hazard assessment in the South China Sea. *Natural Hazards and Earth System Sciences*, *19*(7), 1565–1583. https://doi.org/10.5194/nhess-19-1565-2019

Ren, Y., Wen, R., & Song, Y. (2014). Recent progress of tsunami hazard mitigation in China. *Episodes*, *37*(4), 277–283. https://doi.org/10.18814/epiiugs/2014/v37i4/007

Shinozaki, T. (2021). Geochemical approaches in tsunami research: Current knowledge and challenges. *Geoscience Letters*, *8*(1), 6. https://doi.org/10.1186/s40562-021-00177-9

Sun, L., Zhou, X., Huang, W., Liu, X., Yan, H., Xie, Z., et al. (2013). Preliminary evidence for a 1000-year-old tsunami in the South China Sea. *Scientific Reports*, *3*(1), 1655. https://doi.org/10.1038/srep01655

Tan, L., Zhou, Y., Song, C., Xing, L., Zhu, L.-H., Wang, N., et al. (2025). A 400-year sediment record of tsunamis in Qi'ao Island, centered at Guangdong-Hong Kong-Macao greater Bay area [Dataset]. *Figshare*. https://doi.org/10.6084/m9.figshare.29858489.v1

Wang, X., Guo, Y., & Ren, J. (2021). The coupling effect of flood discharge and storm surge on extreme flood stages: A case study in the pearl river Delta, South China. *International Journal of Disaster Risk Science*, *12*(4), 1–15. https://doi.org/10.1007/s13753-021-00355-5

Wang, X., & Power, W. L. (2011). *COMCOT: A tsunami generation propagation and Run-Up model*. Cornel University, Cornel University.

Wang, Y., Wang, Y., Li, L., Xu, Y., Chen, X., & Zhang, P. (2023). Paleo-tsunami sedimentary records and potential triggering mechanism during the earlier Song dynasty at the northern South China Sea. *Chinese Science Bulletin*, *68*(20), 2690–2708. (in Chinese). https://doi.org/10.1360/TB-2022-1137

Watanabe, M., Goto, K., Bricker, J. D., & Imamura, F. (2018). Are inundation limit and maximum extent of sand useful for differentiating tsunamis and storms? An example from sediment transport simulations on the sendai plain, Japan. *Sedimentary Geology*, *364*, 204–216. https://doi.org/10.1016/j.sedgeo.2017.12.026

Xia, S., Zhou, P., Zhao, D., & Cao, J. (2020). Seismogenic structure in the source zone of the 1918 M7.5 NanAo earthquake in the northern South China Sea. *Physics of the Earth and Planetary Interiors*, *302*, 106472. https://doi.org/10.1016/j.pepi.2020.106472

Xiao, S., Li, A., Jiang, F., Li, T., Huang, P., & Xu, Z. (2005). Recent 2000-year geological records of mud in the inner shelf of the East China Sea and their climatic implications. *Chinese Science Bulletin*, *50*(5), 466–471. https://doi.org/10.1007/BF02897464

Xing, L., Zhang, H., Yuan, Z., Sun, Y., & Zhao, M. (2011). Terrestrial and marine biomarker estimates of organic matter sources and distributions in surface sediments from the East China Sea shelf. *Continental Shelf Research*, *31*(10), 1106–1115. https://doi.org/10.1016/j.csr.2011.04.003

Xiong, H., Zong, Y., Qian, P., Huang, G., & Fu, S. (2018). Holocene sea-level history of the northern coast of South China Sea. *Quaternary Science Reviews*, *194*, 12–26. https://doi.org/10.1016/j.quascirev.2018.06.022

Yang, W., Sun, L., Yang, Z., Gao, S., Gao, Y., Shao, D., et al. (2019). Nan'ao, an archaeological site of Song dynasty destroyed by tsunami. *Chinese Science Bulletin*, *64*(1), 107–120. (in Chinese). https://doi.org/10.1360/N972018-00740

Yao, Q., Liu, K.-b., Zhang, Z., Rodrigues, E., Cohen, M., Maiti, K., & Yang, Y. (2023). What are the Most effective proxies in identifying storm-surge deposits in paleotempestology? A quantitative evaluation from the Sand-Limited, peat-dominated environment of the Florida coastal everglades. *Geochemistry, Geophysics, Geosystems*, *24*(3), e2022GC010708. https://doi.org/10.1029/2022GC010708

Yoneda, M., Uno, H., Shibata, Y., Suzuki, R., Kumamoto, Y., Yoshida, K., et al. (2007). Radiocarbon marine reservoir ages in the western Pacific estimated by pre-bomb molluscan shells. *Nuclear Instruments and Methods in Physics Research Section B: Beam Interactions with Materials and Atoms*, *259*(1), 432–437. https://doi.org/10.1016/j.nimb.2007.01.184

Yu, F., Zong, Y., Lloyd, J. M., Huang, G., Leng, M. J., Kendrick, C., et al. (2010). Bulk organic δ13C and C/N as indicators for sediment sources in the Pearl River delta and estuary, southern China. Estuarine. *Coastal and Shelf Science*, *87*(4), 618–630. https://doi.org/10.1016/j.ecss.2010.02.018

Yu, K.-F., Zhao, J.-X., Shi, Q., & Meng, Q.-S. (2009). Reconstruction of storm/tsunami records over the last 4000 years using transported coral blocks and lagoon sediments in the southern South China Sea. *Quaternary International*, *195*(1–2), 128–137. https://doi.org/10.1016/j.quaint.2008.05.004

Zhang, J., Li, P., Tomczak, M., Wang, Y., Gan, H., Cai, G., et al. (2024). Diatom record the holocene marine facies deposition history in inner Bay of Pearl River Estuary, South China. Estuarine. *Coastal and Shelf Science*, *302*, 108766. https://doi.org/10.1016/j.ecss.2024.108766

Zheng, L.-W., Ding, X., Liu, J. T., Li, D., Lee, T.-Y., Zheng, X., et al. (2017). Isotopic evidence for the influence of typhoons and submarine canyons on the sourcing and transport behavior of biospheric organic carbon to the deep sea. *Earth and Planetary Science Letters*, *465*, 103–111. https://doi.org/10.1016/j.epsl.2017.02.037

Zhou, L., Yang, Y., Wang, Z., Jia, J., Mao, L., Li, Z., et al. (2019). Investigating ENSO and WPWP modulated typhoon variability in the South China Sea during the mid–late Holocene using sedimentological evidence from southeastern Hainan Island, China. *Marine Geology*, *416*, 105987. https://doi.org/10.1016/j.margeo.2019.105987

Zhu, Y., An, C., Yu, H., Zhang, W., & Chen, X. (2024). High-resolution tsunami hazard assessment for the Guangdong-Hong Kong-Macao greater Bay area based on a non-hydrostatic tsunami model. *Science China Earth Sciences*, *67*(7), 2326–2351. https://doi.org/10.1007/s11430-023-1300-9

Zong, Y., Yu, F., Huang, G., Lloyd, J. M., & Yim, W. W. S. (2010). Sedimentary evidence of late Holocene human activity in the pearl river delta, China. *Earth Surface Processes and Landforms*, *35*(9), 1095–1102. https://doi.org/10.1002/esp.1970

References From the Supporting Information

Burroughs, S. M., & Tebbens, S. F. (2005). Power-law scaling and probabilistic forecasting of tsunami runup heights. *Pure and Applied Geophysics*, *162*(2), 331–342. https://doi.org/10.1007/s00024-004-2603-5

Hui, C., Ning, L., & Cheng, C. (2022). Risk assessment of tsunamis along the Chinese Coast due to earthquakes. *International Journal of Disaster Risk Science*, *13*(2), 275–290. https://doi.org/10.1007/s13753-022-00407-4

Kortekaas, S., & Dawson, A. G. (2007). Distinguishing tsunami and storm deposits: An example from Martinhal, SW Portugal. *Sedimentary Geology*, *200*(3–4), 208–221. https://doi.org/10.1016/j.sedgeo.2007.01.004

Wang, F., Yang, B., Tian, L., Li, J., Shang, Z., Chen, Y., et al. (2016). The choice of CIC and CRS models of 210Pbexc dating for tidal flat area. *Earth Science - Journal of China University of Geosciences*, *41*(6), 971–981. (in Chinese). https://doi.org/10.3799/dqkx.2016.081

19448007, 2025, 19, Downloaded from https://agupubs.onlinelibrary.wiley.com/doi/10.1029/2025GL117291 by Ocean University Of China, Wiley Online Library on [03/10/2025]. See the Terms and Conditions (https://onlinelibrary.wiley.com/terms-and-conditions) on Wiley Online Library for rules of use; OA articles are governed by the applicable Creative Commons License